CHAPTER 5

DENDRITIC GROWTH OF POLY(ε-CAPROLACTONE) CRYSTALS FROM COMPATIBLE BLENDS WITH POLY(t-BUTYL ACRYLATE) AT THE AIR/WATER INTERFACE

5.1. Abstract

Thermodynamic analyses of surface pressure-area (Π-A) isotherms and Brewster angle microscopy (BAM) reveal that poly(ε-caprolactone) (PCL) and poly(t-butyl acrylate) (PtBA) form compatible blends as Langmuir films below the dynamic collapse transition for PCL at a surface pressure of ~ 11 $mN \cdot m^{-1}$. For PCL-rich blends, *in situ* BAM studies reveal dendritic growth of PCL crystals in the plateau regime of the Π-A isotherm. These diffusion limited structures presumably arise from the exclusion of PtBA from the growing PCL crystals and hindered diffusion of PCL from the surrounding monolayer to the crystal growth fronts. The ability to transfer the PCL dendrites as Langmuir-Schaefer films onto silicon substrates coated with a spincoated polystyrene layer facilitates detailed morphological characterization by optical and atomic force microscopy (AFM). AFM reveals that the dendritic branching is at angles of ~80° and ~50° along the {100} and {110} sector boundaries and is essentially independent of composition. AFM also reveals that the crystal thickness of PCL dendrites, ~ 7 to 8 nm, is comparable to PCL crystals grown from single-component PCL Langmuir films. In contrast, PtBA-rich blend films suppress PCL crystallization. These findings establish PCL blends as ideal systems for exploring diffusion-limited growth of semicrystalline polymers in two-dimensional confined geometries.

5.2. Introduction

Previous studies on polymers confined in thin film geometries have attracted widespread interest because of their potential applications in semiconductors,[145, 146] antireflection coatings,[147] electrochemical devices,[148] and drug delivery systems.[149] In particular, thin film crystallization of semicrystalline polymers has drawn significant attention for understanding the properties of thin film materials. Decreasing film thickness dramatically alters molecular mobility,[4, 5] glass transition temperatures,[6, 7] and chain orientation[8-10, 145] of semicrystalline polymers. These factors influence the transport of chain segments to the growth fronts of crystallizing lamellae, resulting in growth rates, degrees of crystallinity, morphologies and melting behavior that differ from bulk crystals.[8-23] Moreover, the reduction in dimensionality in going from a three-dimensional (3D) to quasi-two dimensional (2D) system further limits the amount of crystallizable material in the vicinity of the growth front. This effect is consistent with previous studies that observe diffusion-limited crystal growth in polymer thin films below a certain threshold thickness value.[9, 12-19, 118] Previously observed diffusion-limited morphologies include dense-branched morphologies, dendrites, and fractal structures.[9, 12-19, 118]

One of the most heavily studied crystallizable polymers for thin film studies is poly(ethylene oxide) (PEO). Dendritic crystals of PEO have been observed as PEO film thickness approaches ~ 10 nm in contrast to single crystal and spherulitic morphologies observed in thicker films.[19, 118] Furthermore, adding amorphous poly(methylmethacrylate) (PMMA) into PEO has been used to "tune" the crystal morphology of PEO in mixed thin films.[19, 118] The morphologies of the blends were found to shift from spherulites, to needles, and dendrites as the composition decreased

from 90 to 30 wt% PEO.[118] In addition, adding a fixed amount of clay (5 wt% relative to the total polymer mass) to PEO/PMMA blends yields seaweed dendritic growth (50 wt% PEO), symmetric dendritic growth (30 wt% PEO), and fractal dendritic growth (20 wt% PEO).[19] Moreover, previous studies also suggest that both crystallization temperature and blend composition play similar roles on the morphological evolution of PEO crystals in PEO/PMMA blend films because both parameters alter the diffusive properties (diffusion coefficient, diffusion length, etc.) of the crystalline component.[19, 118]

Polymer crystallization in thin film geometries is not limited to studies of PEO. Taguchi *et al.* extensively investigated the crystal growth of isotactic polystyrene (it-PS) in ~ 11 nm thick film.[122] Sixfold symmetric dendrites and compact seaweedlike dendrites were observed with decreasing crystallization temperature. Similar diffusion-limited morphologies have also been reported for other polymer systems such as poly(styrene-ethyleneoxide),[15] poly(trifluoroethylene),[123] poly(ethylene terephthalate),[124] and poly(S-lactide).[122]

Another system, poly(ε-caprolactone) (PCL), is frequently used as a model semicrystalline polymer and will be used in this study. PCL is a hydrophobic polyester with a bulk glass transition temperature of T_g ~ -60 ^oC, a melting point of T_m ~ 50 ^oC, excellent biocompatibility, and low toxicity. In the past decade, PCL based systems have attracted considerable interest for controlled-release drug delivery[151-153] and as scaffolds for tissue engineering[154-162] that require a fundamental understanding of PCL's degradation mechanisms and crystallization behavior.[76] For thin film geometries, crystallization of PCL and PCL-based polymer blends have recently been studied.[8-10] The growth rate of PCL crystals was found to be roughly one-half the bulk growth rate at

crystallization temperatures of 50 °C and 54 °C for 15 nm thick films.[9] In contrast, 6 nm thick films exhibit drastically slower growth rates which are comparable at both temperatures. However, as film thickness increases, bulk crystallization rates are recovered. For example, the growth rates observed for PCL films with thicknesses in the range of 30-200 nm at both 50 °C and 54 °C are consistent with measurements for thicker films up to 2000 nm and bulk crystallization.[8-10] Like the PEO case discussed above, dendritic morphologies are also observed in 6 nm or thinner PCL spincoated films on silicon substrates.[9]

For the aforementioned studies on thin film crystallization, the polymer films are usually prepared on solid substrates by spincoating. The cooperative motion of polymer chains on solid substrates directly affects chain folding and consequently the crystallization rate and morphology. Furthermore, surface defects on solid substrates can affect the nucleation mechanism for crystal growth. However, at the air/water (A/W) interface, ultrapure water minimizes surface defects, providing a model surface for probing crystallization in thin films.[24, 26] Even though the growth of dendritic patterns in supersaturated Langmuir monolayers have been evaluated for small amphiphilic molecules such as dioctadecylamine (DODA),[131] ethyl palmitate (EP),[131] ethyl stearate (ES),[131] diacetylene 10, 12-tricosadiynoic acid,[132] D-myristol alanine,[133, 134] and N-dodecylgluconamide,[53] to the best of our knowledge, diffusion-limited growth of polymer crystals in Langmuir monolayers has only been observed for PCL-based systems.[24, 26] In previous studies, we reported that PCL Langmuir films formed at low surface pressures exhibit the nucleation of crystals at room temperature (T = 22.5 °C) from a meta-stable (supersaturated) monolayer at surface pressures (Π) just below the dynamic collapse

pressure of $\Pi_{C,PCL} \sim 11$ mN·m^{-1}.[24, 26] The growth of crystals in the subsequent plateau regime of the surface pressure-area per repeating unit (monomer for short, Π-A) isotherm was observed by *in situ* Brewster angle microscopy (BAM) studies. Electron diffraction studies on Langmuir-Schaefer (LS) films indicate that the lamellar crystals are oriented with the polymer chain axes perpendicular to the substrate surface, while atomic force microscopy (AFM) reveals a crystal thickness of ~ 8 nm.[24] In addition, a molar mass dependent collapse transition for PCL monolayers was observed in both dynamic compression and "equilibrium" addition experiments.[26] Molar mass dependent morphological features of PCL crystals and their subsequent crystal melting were also observed by *in situ* BAM studies during hysteresis experiments.[26]

In this study, PCL (weight average molar mass, M_w = 10 kg•mol^{-1}) is blended with amorphous poly(*t*-butyl acrylate) (PtBA) (M_w = 25.7 kg•mol^{-1}, bulk $T_g \sim 36$ ^{o}C). The compatibility and rigidity of these blends in the monolayer regime is analyzed through the Wilhelmy plate technique and BAM. Morphological changes arising from the enhanced rigidity and hindered transport of PCL to the growth fronts of crystals during dynamic compression experiments, and the melting of crystals during dynamic hysteresis experiments are examined *in situ* by BAM. A more extensive analysis of PCL dendrites formed in Langmuir films is obtained from optical microscopy (OM) and AFM studies performed on LS-films prepared on silicon substrates coated with polystyrene. Collectively, these measurements provide insight into the crystallization of polymers in constrained systems that approach 2D as closely as possible.

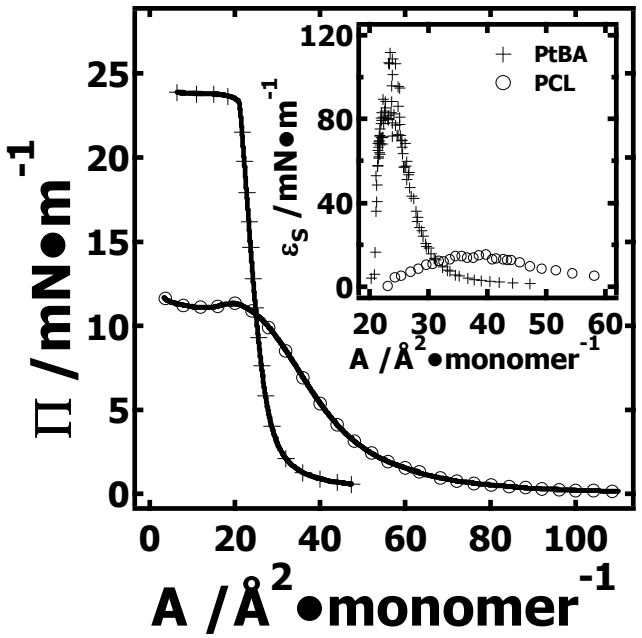

Figure 5.1. Π–A compression isotherms for M_w = 10 kg•mol^{-1} PCL (○) and M_w = 25.7 kg•mol^{-1} PtBA (+) at the A/W interface. The isotherms were obtained at T = 22.5 °C and a compression rate of 8 cm^2·min^{-1}. The inset shows ε_s values deduced from the isotherms as a function of A.

5.3. Results and Discussion

5.3.1. Compression Isotherm Studies for PCL and PtBA Langmuir Films

Figure 5.1 shows Π-A isotherms for PCL and PtBA at the air/water (A/W) interface at a temperature of T = 22.5 °C. The isotherms for the single component PCL and PtBA Langmuir films are consistent with previous studies.[24-26, 75, 163-165] Starting with PCL, the monolayer exhibits a gentle change in Π from 0 at A ~ 140 Å^2·monomer^{-1} (not shown) to ~ 11.3 mN·m^{-1} at A ~ 20 Å^2·monomer^{-1}. The gentle rise in Π is characteristic of a compressible film, and the isotherm can be used to calculate the 2D analog to the bulk

modulus, the static dilational elasticity, $\varepsilon_s = \kappa^{-1} = -A(\partial\Pi/\partial A)_T$, where κ is the 2D analog of the bulk isothermal compressibility.[166-168] ε_s values for PCL as a function of A are provided in the inset of Figure 5.1. As seen in Figure 5.1, ε_s exhibits a maximum value, $\varepsilon_{s,max,PCL} \sim 14$ mN·m^{-1} at A ~ 37 Å^2·monomer^{-1}. $\varepsilon_{s,max,PCL}$ is consistent with PCL forming a liquid-expanded (LE) monolayer.[24, 26, 166-168] For A < 20 Å^2·monomer^{-1}, the PCL isotherm exhibits a kink in the isotherm followed by a plateau that is indicative of film "collapse". The kink yields a dynamic collapse pressure of $\Pi_{C,PCL} \sim 11.3$ mN·m^{-1}. As previously reported, "collapse" of the PCL monolayer during dynamic compression experiments corresponds to the nucleation and growth of crystals from a supersaturated monolayer.[24, 26]

Switching to the PtBA Π-A isotherm, PtBA initially shows a gentle rise in Π until ~ 2 mN·m^{-1} at A ~ 32 Å^2·monomer^{-1} that is similar to PCL. However, further compression of the PtBA film causes Π to rise much more sharply for PtBA than for PCL indicating that PtBA is substantially less compressible. In fact, the maximum static dilational elasticity for PtBA, $\varepsilon_{s,max,PtBA} \sim 110$ mN·m^{-1} at ~ 23.4 Å^2·monomer^{-1}, is consistent with a liquid condensed (LC) monolayer.[164, 167, 168] For A < ~ 21Å^2·monomer^{-1}, the PtBA monolayer undergoes collapse into multilayer structures at a dynamic collapse pressure of $\Pi_{C,PtBA} \sim$ 23 mN·m^{-1}.[62, 63] On the basis of Figure 5.1, the addition of PtBA to PCL should enhance the rigidity of the resulting Langmuir film, and the $\Pi_{C,PCL}$ value means that any analysis of monolayer compatibility needs to be restricted to $\Pi < \Pi_{C,PCL}$.

5.3.2. Compression Isotherm Studies for PCL/PtBA Langmuir Film Blends

Figure 5.2 contains Π-<A> isotherms for PCL blends with PtBA at various mole fractions of PtBA, X_{PtBA}. X_{PtBA} values in this paper are calculated on the basis of the molar mass of the repeating units rather than the molar masses of the entire polymer chain. Examination of Figure 5.2 clearly reveals two important regimes: $\Pi < \Pi_{c,PCL}$ and $\Pi > \Pi_{c,PCL}$. For the higher Π region, $\Pi_{c,PtBA}$ is essentially constant and one is simply observing the effect of diluting PtBA with PCL that has already undergone "collapse" – crystallization or the formation of amorphous multilayer domains depending on X_{PtBA} (to be discussed below). In the lower Π region, one observes that the blends show a systematic shift from single-component PCL behavior to single-component PtBA behavior as X_{PtBA} increases. This region of the film corresponds to the Langmuir monolayer and can be used to determine the excess Gibbs free energy of mixing, ΔG_{excess}.

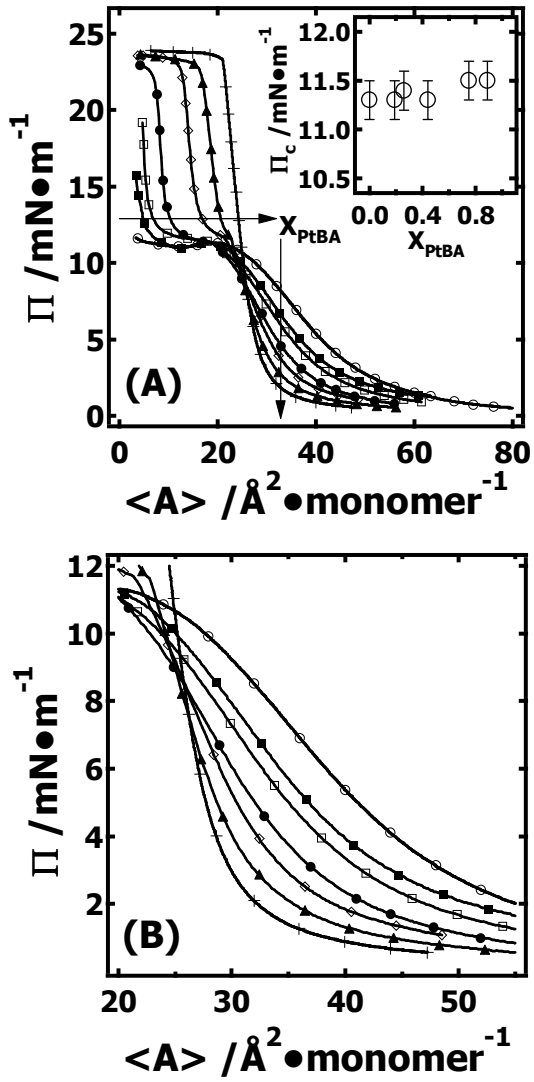

Figure 5.2. (A) Π–<A> compression isotherms for various PCL/PtBA blends at the A/W interface. The isotherms were obtained at T = 22.5 °C and a compression rate of 8 $cm^2 \cdot min^{-1}$ and correspond to X_{PtBA} = 0 (PCL, ○), 0.19 (■), 0.26 (□), 0.44 (●), 0.75 (◊), 0.89 (▲), and 1.0 (PtBA, +). The inset highlights the essentially composition independent value of the dynamic $\Pi_{C,PCL}$. The arrows on (A) indicate the trend of increasing X_{PtBA}. (B) The same isotherms in (A) are expanded to clearly show the monolayer regime.

In order to determine ΔG_{excess} for a binary mixture of PCL and PtBA in the monolayer regime, one starts with the area additivity rule for an ideal mixture:[48(c, e, g)]

$$\left\langle A_{mix,ideal}(\Pi)\right\rangle = X_{PCL}A_{PCL}(\Pi) + X_{PtBA}A_{PtBA}(\Pi) \quad (5\text{-}1)$$

where the X_{PCL} and X_{PtBA}, and $A_{PCL}(\Pi)$ and $A_{PtBA}(\Pi)$ correspond to the mole fractions and areas per monomer of the pure components at specific Π values, respectively. Eq. 5-1 then allows one to calculate the area change upon mixing, the 2D analog of the change in volume upon mixing in 3D:

$$\Delta A_{mix}(\Pi) = \left\langle A(\Pi)\right\rangle - \left\langle A_{mix,ideal}(\Pi)\right\rangle \quad (5\text{-}2)$$

where $<A(\Pi)>$ corresponds to the experimental values in Figure 5.2. Figure 5.3A shows a comparison of $<A_{mix,ideal}(\Pi)>$ with $<A(\Pi)>$ as a function of X_{PtBA} for different Π from 2 to 10 $mN\cdot m^{-1}$. As seen in Figure 5.3A, all mixtures show strongly negative deviation from ideal mixing at all X_{PtBA} and Π. ΔG_{excess} can be obtained from Eq. 5-2 through

$$\Delta G_{excess}(\Pi) = \int_o^{\Pi} \Delta A_{mix}(\Pi) d\Pi \quad (5\text{-}3)$$

Figure 5.3B shows ΔG_{excess} vs. X_{PtBA} at the same Π as in Figure 5.3A. For all Π and X_{PtBA}, ΔG_{excess} is strongly negative indicating that PtBA and PCL are compatible in the monolayer regime. This conclusion is supported by BAM images which are homogeneous for $\Pi < \Pi_{C,PCL}$.

The isotherms in Figure 5.2 can also be evaluated by considering the monolayer to be a 2D semi-dilute solution. During the 1980's, researchers in the field noted that in the semi-dilute monolayer regime, Π was molar mass independent and scaled with surface concentration as $\Pi \sim \Gamma^z$ or $\Pi \sim A^{-z}$.[166, 169-170] More recently, Esker *et al.* noted that if one assumed $\Pi \sim 0$ at the start of the semi-dilute regime, one obtained, $\varepsilon_s = z\Pi$.[167, 168] Hence,

the initial slope of an ε_s-Π plot, provides insight into interactions between water and the polymer through good solvent scaling predictions (z = 3 for a mean field model and z = 2.86 for numerical models)[171, 172] where chains have a solvent swollen 2D conformation, and predictions for theta solvent conditions (z approaches infinity in a mean field model with predictions of z = 8 to 101 from different numerical methods)[59, 60, 173, 174] where the excluded volume of the 2D conformation matches the unperturbed 2D chain conformation. These predictions were consistent with the measurements of dynamic dilational elasticity obtained by Esker *et al.* from surface light scattering.[166] Li *et al.* recently showed that the A/W interface is a good solvent for PCL through this analysis scheme.[24, 26] For PtBA, the similarity of the structure and shape of the Π-A isotherm with poly(t-butylmethacrylate) would suggest that PtBA should be close to the theta solvent limit.

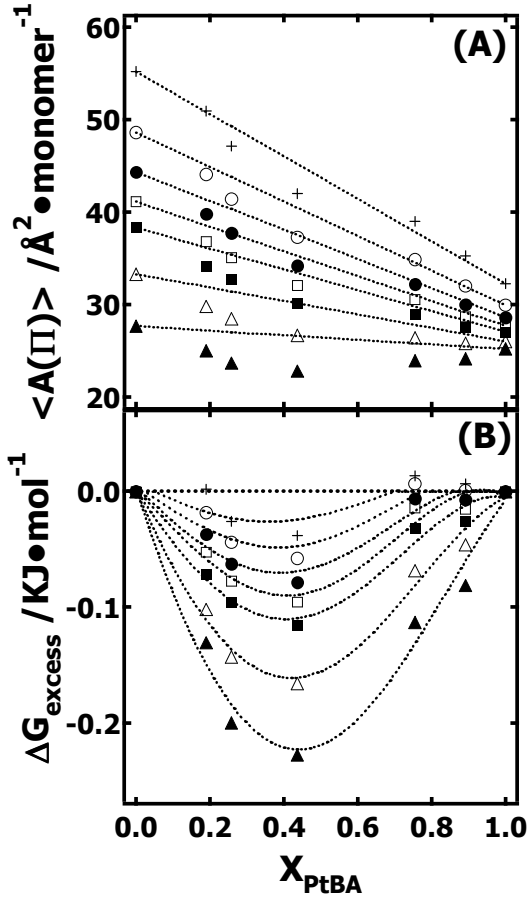

Figure 5.3. (A) <A(Π)> obtained from the isotherms in Figure 5.2 as a function of X_{PtBA} for various PCL/PtBA blends: Π = 2 (+), 3 (○), 4(●), 5 (□), 6 (■), 8 (Δ), and 10 (▲) $mN \cdot m^{-1}$. The dotted lines correspond to $<A_{mix,ideal}(\Pi)>$ from Eq. 5-1 in the order of lowest to highest Π from the top to the bottom of the plot. Negative deviation from the area additivity rule is observed for all Π. (B) ΔG_{excess} obtained from Eq. 5-3 as a function of X_{PtBA} for the same Π values used in (A). The dotted lines are only provided to highlight the trend of increasing ΔG_{excess} with increasing Π, and the dotted horizontal line is provided to accentuate where $\Delta G_{excess} = 0$.

Figure 5.4A shows ε_s vs. <A> for PCL/PtBA blends at various compositions. In contrast to the pure components (inset of Figure 5.1), the blends show two elasticity maxima, $\varepsilon_{s,max}$, in two distinct regions $\varepsilon_{s,max,1}$ for A > ~ 22 $Å^2$·monomer^{-1} ($\Pi < \Pi_{C,PCL}$, monolayer) and $\varepsilon_{s,max,2}$ for A < ~ 22 $Å^2$·monomer^{-1} ($\Pi > \Pi_{C,PCL}$). Because of the limited compression ratio of our Langmuir trough, it was not possible to obtain both maxima for the two lowest X_{PtBA} in a single experiment. The region corresponding to the Langmuir monolayer state for the blends is expanded as the inset in Figure 5.4A. Table 5.1 summarizes the values of $\varepsilon_{s,max,1}$, and $\varepsilon_{s,max,2}$ and the <A> values where they occur, $<A(\varepsilon_{s,max,1})>$ and $<A(\varepsilon_{s,max,2})>$, respectively, for each X_{PtBA}. For A < ~ 22 $Å^2$·monomer^{-1} ($\Pi > \Pi_{C,PCL}$) the PCL component has "collapsed" – crystallization or the formation of amorphous multilayer domains depending on X_{PtBA}. In this regime the observed behavior arises from PtBA that remains at the A/W interface following the "collapse" of PCL. Nonetheless, the PCL plasticizes the PtBA that remains at the A/W interface leading to progressively smaller $\varepsilon_{s,max,2}$ at smaller $<A(\varepsilon_{s,max,2})>$ as shown in Figure 5.4A and summarized in Table 5.1. As this region of the isotherm is not the focus of this paper, it will not be discussed further.

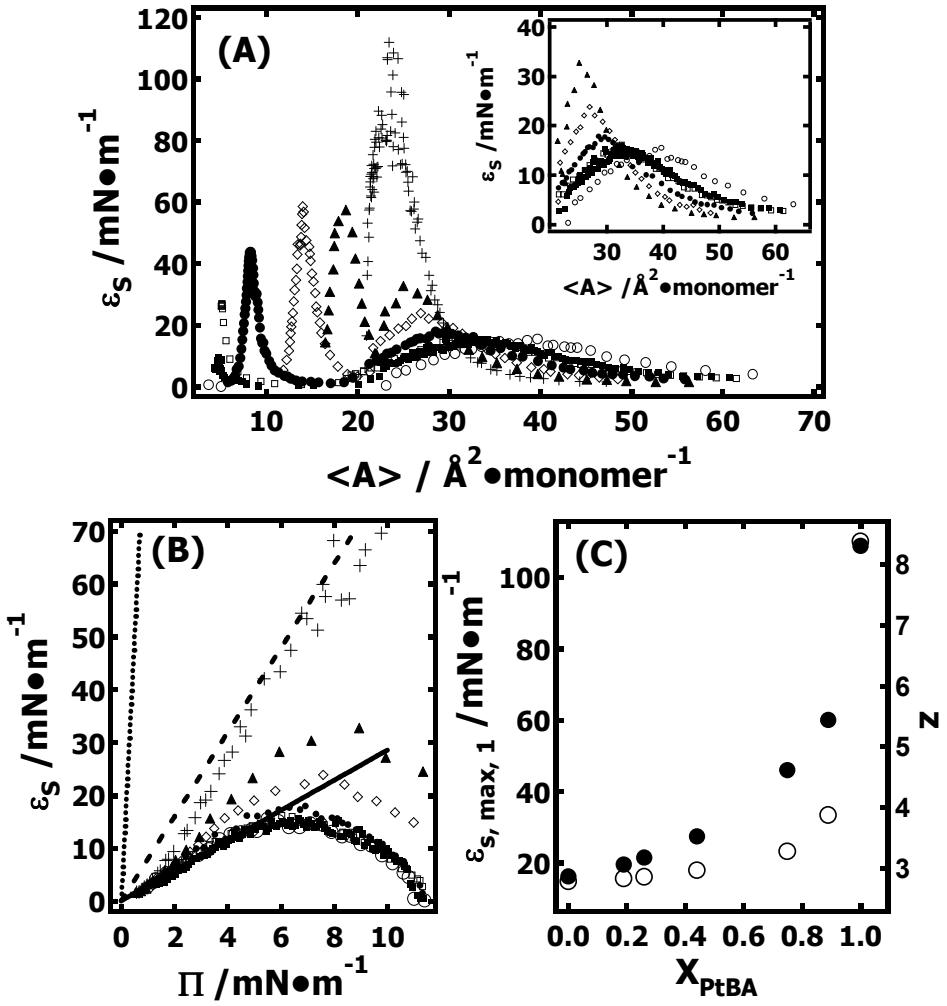

Figure 5.4. (A) ε_s vs. <A> curves for binary PCL/PtBA blends at the A/W interface. ε_s was calculated from the isotherms in Figure 5.2. The inset of (A) focuses on the behavior in the monolayer, $\Pi < \Pi_{C,PCL}$ (PtBA has been excluded for clarity). (B) ε_s vs. Π for binary PCL/PtBA blends. The lines are theoretical curves, $\varepsilon_s = z\Pi$, for good solvent conditions (z = 2.86, solid line),[171] the least extreme numerical value for theta solvent conditions (z = 8, dashed line)[172] and the most extreme numerical value reported for theta solvent conditions (z = 101, dotted line).[59] The symbols in (A) and (B) correspond to X_{PtBA} = 0 (PCL, ○), 0.19 (■), 0.26 (□), 0.44 (●), 0.75 (◊), 0.89 (▲), and 1.0 (PtBA, +). (C) $\varepsilon_{s,max,1}$ vs. X_{PtBA} (open symbols, left-hand axis) obtained from the inset of 5.4A and z vs. X_{PtBA} (filled symbols, right-hand axis) obtained from the initial slope of (B) in the monolayer regime, $\Pi < \Pi_{C,PCL}$. The right- and left-hand axes have been scaled to ensure that z and $\varepsilon_{s,max}$ match for the single-component films.

Focusing on the Langmuir monolayer regime, A > ~ 22 $Å^2$·monomer^{-1} ($\Pi < \Pi_{C,PCL}$), there is a progressive increase in $\varepsilon_{s,max,1}$ and decrease in $<A(\varepsilon_{s,max,1})>$ as X_{PtBA} increases (inset of Figure 5.4A and Table 5.1). As shown in Figure 5.4B, the increase in $\varepsilon_{s,max,1}$ is coupled with a change from good-solvent scaling behavior to poorer (near theta) solvent scaling behavior as the PtBA content of the binary blend films increases. Figure 5.4C shows that neither $\varepsilon_{s,max,1}$ nor z increase linearly as a function of X_{PtBA}, and that z is more sensitive to X_{PtBA} than $\varepsilon_{s,max,1}$ at small X_{PtBA}. The PCL and its attendant water can be thought of as a plasticizer if one considers the monolayer from the perspective of the PtBA component. Nonetheless, as PtBA is added to the film, the rigidity of the monolayer does increase.

Table 5.1. Elasticity maxima for various PCL/PtBA blends.

X_{PtBA}	$<A(\varepsilon_{s,max,1})>$ $Å^2$·monomer^{-1}	$\varepsilon_{s,max,1}$ mN·m^{-1}	$<A(\varepsilon_{s,max,2})>$ $Å^2$·monomer^{-1}	$\varepsilon_{s,max,2}$ mN·m^{-1}
0.00	37.3	14.9	N/A[a]	N/A[a]
0.19	32.8	15.6	4.7	9.6
0.26	31.8	16.1	5.2	26.7
0.44	29.2	18.0	8.3	43.7
0.75	26.3	23.2	14	58.5
0.89	25.0	33.4	18.8	57.4
1.00[b]	23.4	110	23.4	110

[a] Not applicable
[b] While only one maximum is observed for pure PtBA films, the values are listed twice as the PtBA component is responsible for the second peak in the blends.

Having established that PCL/PtBA blends form compatible Langmuir monolayers, and that the rigidity of the film increases with increasing PtBA content, it is necessary to

return to the discussion of Figure 5.2. The inset of Figure 5.2 shows that the dynamic $\Pi_{C,PCL}$ is essentially independent of X_{PtBA}. This feature of the blend system is consistent with Li *et al.*'s observation that $\Pi_{C,PCL}$ corresponds to the "crystallization" pressure for PCL Langmuir films at the A/W interface at 22.5 °C during dynamic compression experiments.[24, 26] In the remainder of this paper, we will focus on how the PtBA component affects the crystallization of PCL through BAM, OM, and AFM studies.

5.3.3. Morphological Studies of PCL Crystallization/Melting in Dynamic Hysteresis Experiments

Li *et al.* recently reported that PCL undergoes crystallization during dynamic compression Π-A isotherms for $\Pi > \Pi_{C,PCL}$ and that both the crystallization and melting of these crystals in dynamic hysteresis experiments is molar mass dependent.[26] In these crystals, the polymer chain axes are perpendicular to the A/W interface and the lamellar thicknesses are on the order of 7 to 8 nm. More recently, work from the Duran group shows that PCL-PEO copolymers can also undergo crystallization in Langmuir films.[163] Figure 5.5 shows representative crystals for PCL grown during a dynamic compression experiment in a Langmuir film (Figure 5.5A), and also shows melting PCL crystals with dendritic morphologies during the expansion of the same monolayer at various A values (Figure 5.5C through E). The Π-A isotherm in Figure 5.5 highlights where the BAM images (Figure 5.5A through E) were taken. The BAM image in Figure 5A shows PCL crystals with four symmetrically distorted {110} sectors and two {100} sectors as indicated in Figure 5B. During the early stages of expansion, PCL in the two {100} sectors immediately starts to melt (Figure 5.5C). This behavior is consistent with observations in single crystals grown in spincoated systems, which Prud'homme *et al.*

attributed to relatively poor organization of the lamellae in the {100} sectors.[9] The lower melting point of the {100} sectors relative to the {110} sectors has also been observed for a single crystal of PLLA with a similar orthorhombic unit cell.[129(a)] The explanation for this difference in melting points is that the direction of the chain folds is parallel to the growth front in the {110} sectors, while the chain folding alternates between the [110] and [1-10] directions in the {100} sectors, leading to less stable chain organization in the {100} sectors. As the crystallized films are further expanded, dendritic arms are observed in the {100} sectors (Figure 5.5D). Similar morphological features are also observed in the OM image (Figure 5.5F) obtained for a LS-film transferred at comparable A during expansion. The schematic in Figure 5.5G highlights the assignment of the {100} and {110} sectors for Figure 5.5F and also is drawn with the same orientation as Figure 5.5B. In the schematic, the solid lines correspond to the orientation of the dendritic sidebranches. Further expansion of the film leads to nearly complete melting of {100} sectors (Figure 5.5E). Four trunks, corresponding to the four boundary lines between {110} and {100} sectors, are the last features to melt as seen in Figure 5.5E. Preferential melting of the different sectors in the single-component PCL films is something that is not clearly observed during the expansion of PCL/PtBA blend films at the A/W interface (to be discussed shortly).

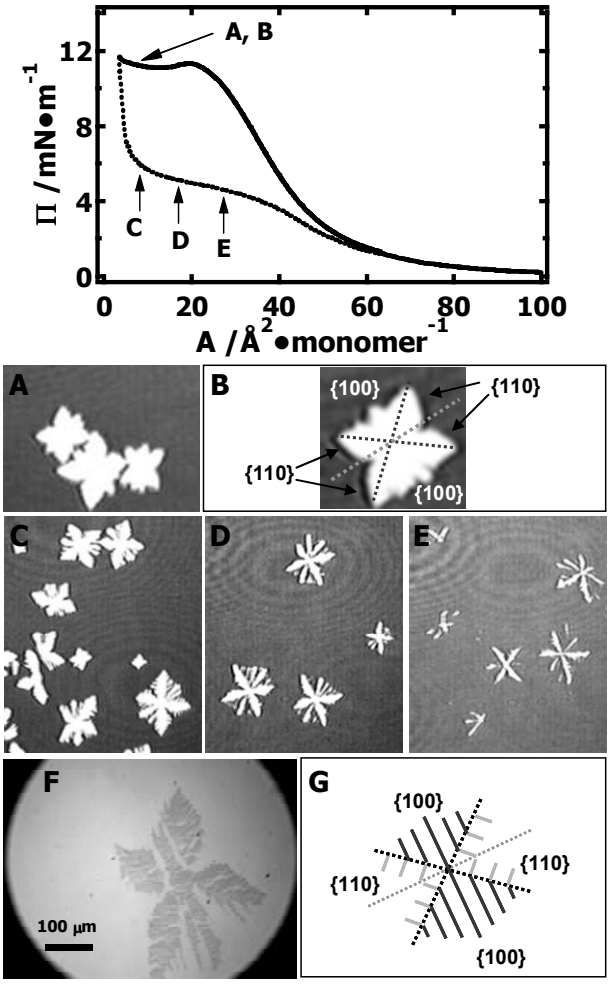

Figure 5.5. (A-E) BAM images for PCL crystals grown from single-component PCL Langmuir films at T = 22.5 ^{o}C and a compression rate of 8 $cm^2 \cdot min^{-1}$. The letters on the Π-A isotherm highlight the surface areas where the BAM images were obtained during compression (A and B) 8 $Å^2 \cdot monomer^{-1}$, and expansion (C – E) 8.2, 17.3, and 27.2 $Å^2 \cdot monomer^{-1}$, respectively. Solid-like domains appear bright in the 1.28 × 0.96 mm^2 image (A) and the 2.0 × 2.4 mm^2 BAM images (C, D, and E). The 0.56 × 0.56 mm^2 BAM image (B) corresponds to an isolated crystal and the principle axes and crystal faces have been added to the crystal. (F) represents an OM image of an LS-film transferred during expansion at A ~ 17 $Å^2 \cdot monomer^{-1}$, a value comparable to the BAM image in (D). (G) An idealized depiction of the PCL dendrites observed during melting drawn with an orientation comparable to the BAM image in (B) and the OM image in (F).

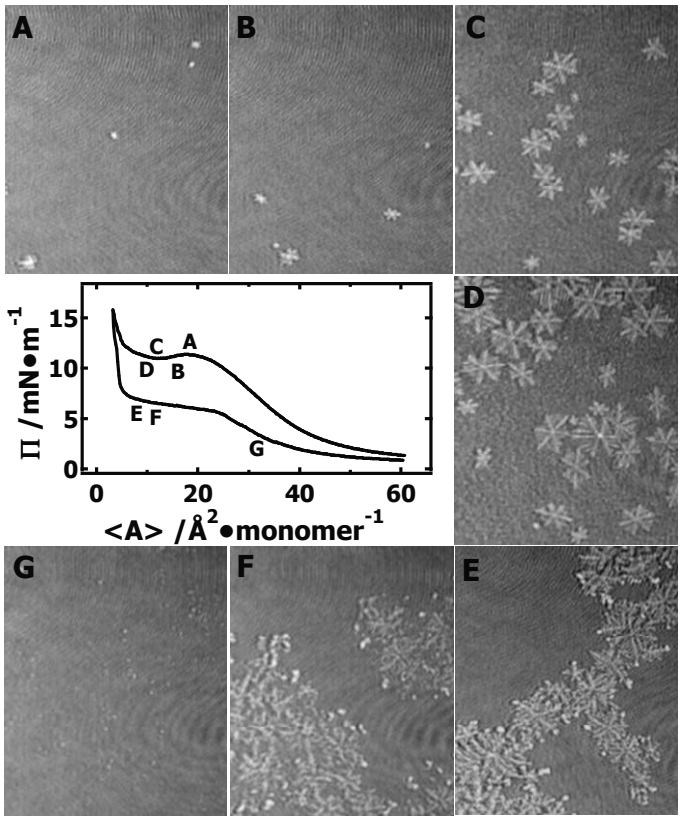

Figure 5.6. BAM images for a X_{PtBA} ~ 0.19 PCL/PtBA blend film obtained at T = 22.5 ^{o}C and a compression and expansion rate of 8 $cm^2 \cdot min^{-1}$. The letters on the isotherm indicate where the BAM images were taken during dynamic hysteresis experiments and correspond to compression (A) 18, (B) 16, (C) 12, and (D) 10 $Å^2 \cdot monomer^{-1}$ and expansion (E) 9.0, (F) 11, and (G) 32 $Å^2 \cdot monomer^{-1}$, of the film. Solid-like domains appear bright in all of the 2.0 × 2.4 mm^2 BAM images.

5.3.4. Morphological Studies of PCL Crystallization/Melting in X_{PtBA} ~ 0.19 PCL/PtBA Blends During Dynamic Hysteresis Experiments

For the M_w = 10 kg·mol^{-1} PCL used in this study, crystallization during dynamic hysteresis experiments at $\Pi > \Pi_{C,PCL}$ show distorted crystals during compression and only exhibit dendritic features during film expansion.[24, 26] In contrast, PCL-rich blends with PtBA exhibit dendritic features even during compression. Figure 5.6 shows representative BAM images for PCL crystals grown and melted at various stages of a dynamic hysteresis experiment for a X_{PtBA} ~ 0.19 PCL/PtBA blend. As noted in the discussion of PCL/PtBA compatibility, all BAM images are homogenous in the monolayer regime prior to compression into the metastable (supersaturated) monolayer regime. Upon compression into the supersaturated monolayer regime, Π close to $\Pi_{C,PCL}$ ~ 11 mN·m^{-1}, small bright domains first appear (not shown here). In this regime, the limited resolution of the BAM image (features > 20 μm can be resolved) means that the only valid conclusion is that nucleation has started. With further compression of the film through the collapse transition for PCL (Figure 5.6A) and into the plateau region of the Π-<A> isotherm, these nuclei grow into larger crystalline domains (Figure 5.6B through D). Even with the limited resolution of the BAM images, it is clear that these crystals exhibit dendritic structures (Figure 5.6B through D). As the PCL crystals grow larger, six-arm dendritic morphologies are more evident (Figure 5.6C and D). In addition to the obvious dendritic crystals, the backgrounds of the images appear to contain very small aggregates that are close in size to the resolution limit of Brewster angle microscope. The nature of these features will be more clearly revealed in subsequent discussion of OM and AFM studies on LS-films prepared in these regions. Continuing with Figure 5.6, the film

is expanded immediately after the compression step by opening the barriers at a constant expansion rate of 8 $cm^2 \cdot min^{-1}$. During the early stages of expansion, the arrangements of PCL chains in the crystals undergo rapid relaxation as the external forces which were applied during compression are removed. As seen in Figure 5.6E, some of the PCL dendritic crystals are broken, possibly as the result of over compression which forces crystal impingement. Further expansion of the film reveals a plateau in the Π-<A> expansion isotherm. This feature is similar to the behavior reported for pure PCL[24, 26] shown in Figure 5.5. The plateau has been attributed to melting of the PCL crystals in a process where the unstable edges diffuse back to the monolayers upon further expansion. During this process, the bright domains become smaller (Figure 5.6F) and their structural details start to disappear in the BAM images as shown in Figure 5.6G. Eventually, these domains become smaller than the 20 μm linear resolution of BAM, and cannot be detected at the end of expansion step.

Another interesting feature of Figure 5.6 is that during the melting process, there does not appear to be a preferential melting of the crystal in different sectors. This behavior is in contrast to the case of the single component PCL film where the {100} sectors melted faster than the better organized {110} sectors. Hence, one possible explanation is that the PCL dendrites in PCL-rich blends may possess uniformly poorer chain organization in all sectors of the PCL crystals in contrast to PCL crystals grown in single-component monolayers.

In order to better understand the morphological features of these PCL dendrites in Figure 5.6, OM and AFM were used to obtain higher resolution images of PCL crystals transferred to silicon substrates coated with a PS layer as LS-films. Figure 5.7 shows a

representative OM image of a single layer LS-film transferred for a $X_{PtBA} \sim 0.19$ PCL/PtBA blend, while Figure 5.8 shows higher resolution AFM images of sidebranching and lamellar thickness. Here, the power of using a PS film to allow the imaging of LS films by shifting interference effects into the visible wavelength range is on full display. First, Figure 5.7 shows the same six-arm dendritic morphology observed in BAM indicating that LS-transfer is suitable for retaining the crystal morphology seen at the A/W interface. Figure 5.7 clearly reveals that the PCL dendrites possess four mirror symmetric dendritic trunks that presumably form along the four boundary lines between the {110} and {100} sectors. Second, the resolution is sufficient to resolve the differences in branching angles (upper insets of Figure 5.7) thereby allowing one to assign the {100} and {110} sectors as done in the lower inset.

The presumed assignment of the {100} and {110} sectors follows the same rationale used by Prud'homme *et al.* for PCL-based thin films on solid surfaces.[9] First, the four mirror-symmetric trunks that define the boundaries between the {110} and {100} sectors have an angle of α less than 90°. Exact measurements of α are complicated by sidebranching in the {100} sectors which causes the arms to bend back to the midline of the {110} sectors as seen in Figure 5.7. Meanwhile, α also appears to depend on the overall size of the crystal. Second, side branches on the two trunks that bisect the {100} sectors experience symmetric growth fields and show a common branching angle of $\gamma = 49.3 \pm 1°$ (analysis in Figure 5.7B). Third, the side branches on the four arms that define the {110} sectors exhibit asymmetric branching angles of $\theta = 77.2 \pm 0.5°$ and $\beta = 51.3 \pm 0.6°$ (analysis in Figure 5.8A'). For sidebranches into the {110} sectors, the branching angle, θ, is nearly perpendicular to the main growth front.

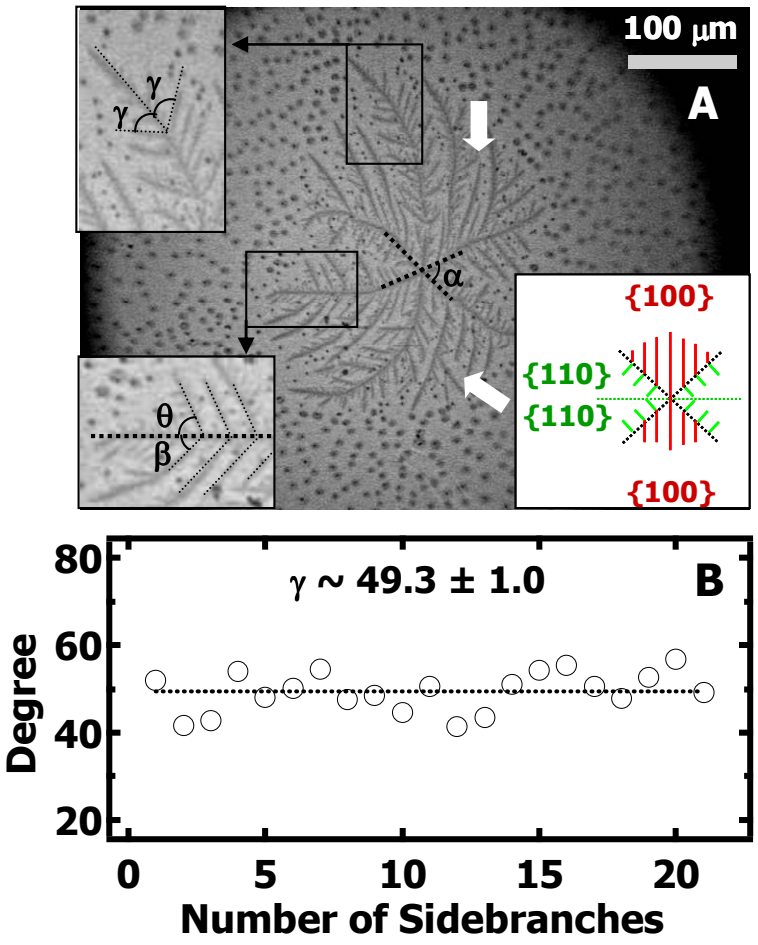

Figure 5.7. (A) A representative OM image of a single layer LS film prepared from a X_{PtBA} ~ 0.19 PCL/PtBA blend film. The LS film was transferred onto a PS coated silicon substrate at <A> ~ 10 $Å^2$·monomer^{-1} during compression in the plateau regime. The inset in the lower right-hand corner shows the assignment of the {100} and {110} sectors with the same orientation as the dendritic crystal in the figure. The inset in the upper left-hand corner shows an enlargement of the symmetric side branching in the {100} sector with a common angle, γ. The inset in the lower left-hand corner shows how θ and β can be resolved by OM along the boundary between a {110} and {100} sector. The white arrows represent regions where the growth of branches is inhibited by side branches from faster growing (earlier forming) branches. (B) The average geometric angle γ vs. the number of sidebranches corresponding to the two dendritic trunks in the two {100} sectors in Figure 5.7A.

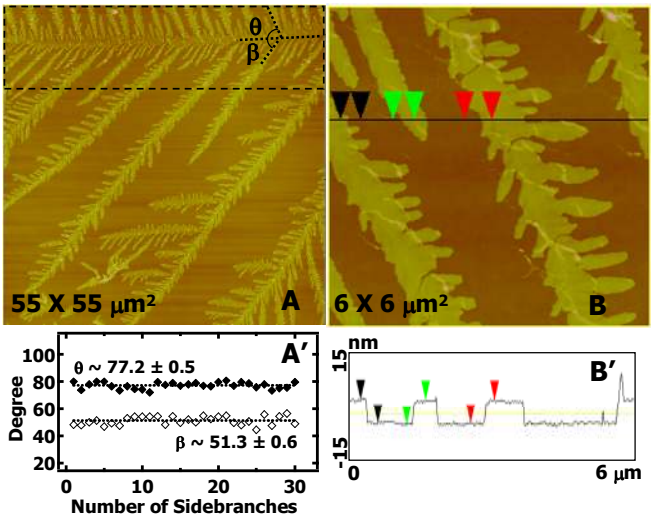

Figure 5.8. Representative AFM images of a single layer LS film for a X_{PtBA} ~ 0.19 PCL/PtBA blend. The LS film was transferred onto a PS coated silicon substrate at <A> ~ 10 $Å^2$·monomer^{-1} in the plateau regime during compression. (A) a 55 × 55 μm^2 height image, (A') the average geometric angles θ and β vs. the number of sidebranches corresponding to the dendritic trunk in the dotted box of (A) that divides a {100} sector from a {110} sector, (B) a 6 × 6 μm^2 height image, (B') a cross-sectional analysis for the solid line in (B). The average thickness of the lamellar crystals is 7.1 nm. Z-scales for images (A) and (B) are 0 to 80 nm and 0 to 60 nm, respectively.

Figures 5.7 and 5.8 have two other significant features. One of these is that the OM image in Figure 5.7 confirms the tenuous conclusion of the low resolution BAM images that the background has small round structures that could be amorphous 3D aggregates. The other is that the lamellar thickness from Figure 5.8 of 7.1 nm is comparable to values for single-component PCL samples crystallized in Langmuir monolayers at the A/W interface.[24, 26]

5.3.5. Effect of X_{PtBA} on PCL Crystal Morphology in PCL/PtBA Blends

In order to understand the effects of X_{PtBA} on PCL crystal morphology, representative BAM and OM images for crystals formed during compression at $\langle A \rangle \sim 10$ Å^2·monomer^{-1} are provided in Figure 5.9. The BAM images, Figures 9A through C show that both the size and number density of dendritic structures decrease with increasing X_{PtBA}. In all three cases, the dendritic crystals exhibit four mirror symmetric {110} sectors and two mirror symmetric {100} sectors. Further analysis of the dendritic crystals by AFM, Figure 5.10, reveals that the characteristic angles β, γ, and θ, along with the lamellar thickness are almost independent of X_{PtBA}. These values are summarized in Table 5.2 for PCL and PCL/PtBA blends. For $X_{PtBA} > 0.44$, PCL crystallization is suppressed and only small clumps of small round structures are observed in AFM images (Figure 5.11). It seems reasonable that these structures could be similar to the 3D aggregates seen in Figure 5.7.

Table 5.2. β , θ, and γ values for PCL dendrites grown from PCL-rich PCL/PtBA belnds.

X_{PtBA}	0.19	0.26	0.44
β	77.2±0.5	79.5±1.0	83.0±0.9
θ	51.3±0.6	50.9±0.9	48.6±1.0
γ	49.3±1.0	48.4±0.8	52.5±1.8

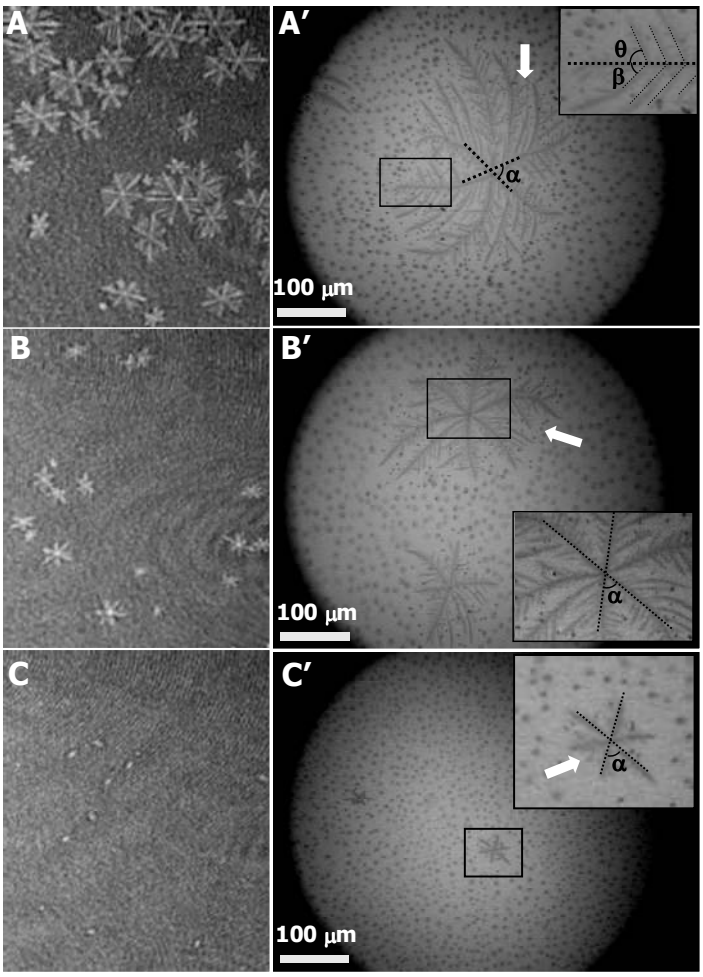

Figure 5.9. PCL crystal morphologies for PCL/PtBA Langmuir film blends with different X_{PtBA} at the A/W interface. The images on the left are BAM images obtained at T = 22.5 °C and an expansion rate of 8 $cm^2 \cdot min^{-1}$ for PCL/PtBA blend films of (X_{PtBA}, <A> /$Å^2 \cdot monomer^{-1}$): (A) (0.19, 10), (B) (0.26, 12), and (C) (0.44, 10). Solid-like domains appear bright in all of the 2.0 × 2.4 mm^2 BAM images. The images on the right, A', B', and C' are OM images for LS films transferred to PS coated silicon wafers at the same conditions as A, B, and C, respectively. The white arrows represent regions where the growth of branches is inhibited by side branches from other faster growing (earlier forming) branches.

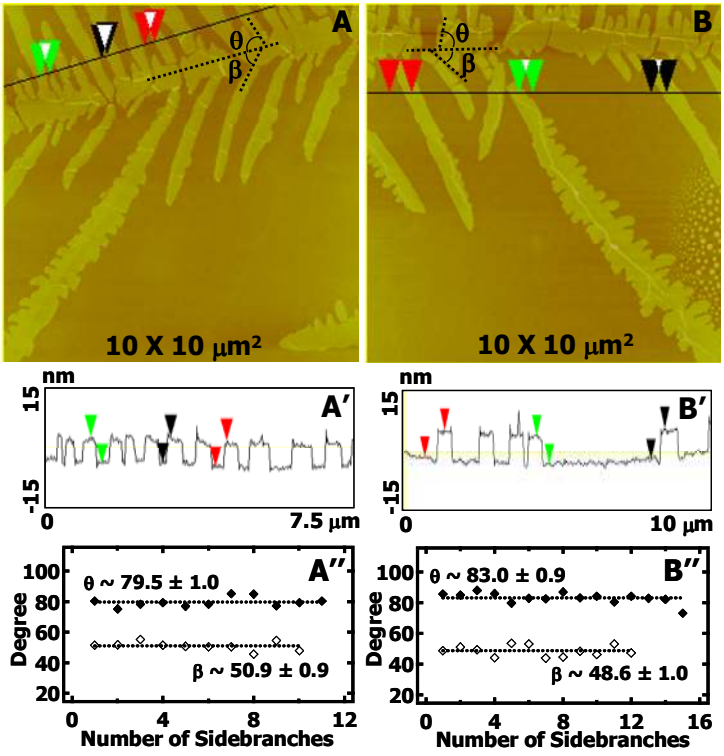

Figure 5.10. AFM height image of a LS film transferred for X_{PtBA} ~ 0.26 and X_{PtBA} ~ 0.44 PCL/PtBA blend films: (A) AFM height image of a LS film transferred for a X_{PtBA} ~ 0.26 PCL/PtBA blend film at <A> ~ 14 $Å^2$·monomer^{-1} (z-scale: 0-60 nm); (A') Cross-sectional analysis for AFM image A (from the solid line on A). The average thickness of the lamellar crystals is 7.1 nm; (A") The average geometric angles θ and β (defined by the dotted lines on A) vs. the number of sidebranches corresponding to the dendritic trunk in image A along a {100} and {110} sector boundary. (B) AFM height image of a LS film transferred for a PCL/PtBA X_{PtBA} ~ 0.44 blend film at <A> ~ 13 $Å^2$·monomer^{-1} (z-scale: 0-60 nm); (B') Cross-sectional analysis for AFM image B (from the solid line on B). The average thickness of the lamellar crystals is 7.5 nm; (B") The average geometric angles θ and β (defined by the dotted lines on B) vs. the number of sidebranches corresponding to the dendritic trunks in image B along the {100} and {110} sector boundary.

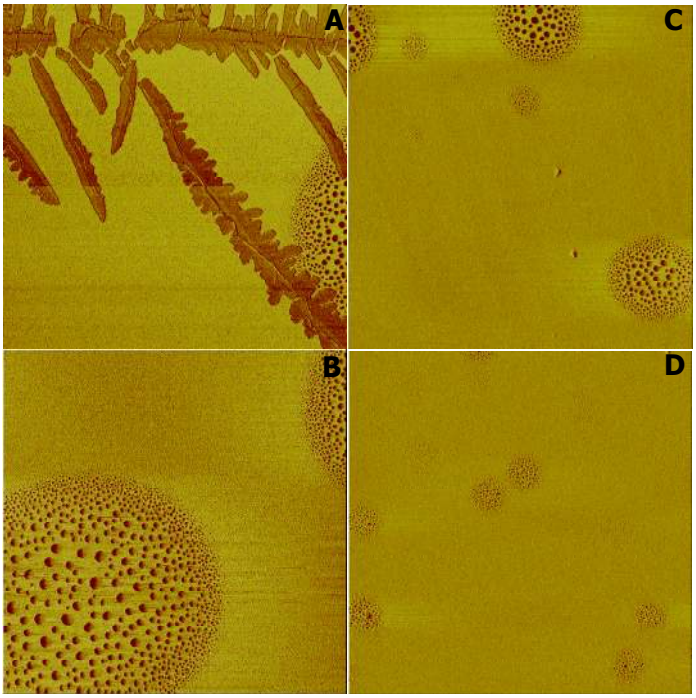

Figure 5.11.AFM phase images of LS films for PCL/PtBA blends: (X_{PtBA}, <A>/Å^2·monomer^{-1}, Π/mN·m^{-1}): (A, B) (0.44, 13, 12); (C) (0.75, 15.6, 14); and (D) (0.89, 20, 14). Softer materials appear darker in all of the 10 ×10 μm^2 AFM images with z-scales of 0-40 deg.

5.3.6. Mechanism for Dendritic Crystallization of PCL in PCL/PtBA Blends During Compression

Dendritic sidebranches normally reflect the symmetry of the crystal structure[175] and grow along crystallographic angles. Examples of this can be found for thin polymer films of PEO/PMMA blends on solid surfaces where fourfold symmetric dendrites form[19, 118] and it-PS where sixfold symmetric dendrites are observed.[122] In general, the diffusion field, either a concentration or temperature gradient at the growth front, causes an interfacial instability in the otherwise flat growth front, leading to the formation of a

protrusion that ultimately gives rise to the formation of dendritic structures.[126, 127] In single-component thin films, it is often assumed that heat transport is not the limiting factor and that the gradient of the film thickness around the growth front is responsible for dendritic crystallization.[122] For blend systems, the compositional instabilities can arise from a non-uniform compositional distribution in blend systems via phase separation, or from diffusion-limited local depletion of crystallizable material and the accumulation of non-crystallizable material that is rejected from the growing crystal at the growth front. Nevertheless, both compositional dendrites and thermal dendrites occur under nonequilibrium conditions.[127] Although dendritic branching for PCL crystals has recently been observed in spincoated films,[9] this chapter is the first report showing the formation of dendritic polymer crystals during compression in homopolymer Langmuir monolayers. As noted by Volhardt *et al.* in studies of dendritic domains in Langmuir films of small molecules, the A/W interface is particularly attractive for studying diffusion-limited pattern formation, because the aqueous phase serves as a large heat sink relative to the single molecule thick films that is capable of quickly dissipating any latent heat thereby ensuring isothermal conditions.[53, 131]

The growth of dendritic structures during the compression of PCL/PtBA blends are comparable to compositional dendrites formed in multi-component systems such as PEO/PMMA.[19, 118] The explanation for the PEO/PMMA system should also be valid for the PCL/PtBA system where adding more rigid PtBA to PCL monolayers hinders the diffusion of PCL chains from the surrounding metastable melt to the crystal growth fronts. At the same time, amorphous PtBA must accumulate in the vicinity of the crystal growth front leading to a local decrease in the supersaturation and a dendritic

morphology. Starting from a stable nuclei, instabilities in the growth front, Mullins-Sekerka instabilites,[126, 127] manifest themselves as protrusions along the six principal trunks of the crystals. Crystal growth is the fastest at the tips of these apexes because the amorphous components are easily rejected from the apexes of the protrusions and the tips experience "virgin" melt. Thus, the semicrystalline component of the blend can preferentially attach on the growth front around the apexes of protrusions. Meanwhile, the accumulation of amorphous components in the vicinity of the protrusions reduces the supersaturation of polymer melt and prevents further growth in the immediate vicinity of the trailing edge of the protrusion. As a result, additional growth behind the leading edge of the tip mainifests itself locally as new protrusions where the supersaturation of crystallizable material has returned to "normal". At these protrusions, the melt is again supersaturated and crystallization takes the form of dendritic branches with fairly uniform branching angles and spacings as seen in Figures 5.7 and 5.8. Once these sidebranches form, further growth is controlled by the local diffusion field around the growth front of the new dendritic tip. Meanwhile, the dendritic branches compete with each other in a limited reservoir of crystallizable polymer. As a result, faster growing branches can cut-off neighboring arms, as indicated by white arrows in Figures 5.7 and 5.9, by locally depleting the crystallizable component. This process, called “kinetic coarsening”, leads to different lengths of sidebranches.[176] The deviations in branch length are more clearly seen in Figure 5.8A. This process may also be responsible for the pronounced bend in the four principal trunks that form the boundaries between the {110} and {100} growth sectors as seen in Figures 5.6 and 5.7. The growth rates of these “secondary” and “tertiary” sidebranches are determined by the overall results of surrounding diffusion

fields, the degree of undercooling, and chain folding with respect to the growth front of dendritic tips, which primarily lead to the morphologies seen in Figures 5.5 through 5.11.

However, kinetic coarsening is not the only process present in the PCL/PtBA system. With increasing X_{PtBA}, the supersaturation is also diminished, and the diffusion is presumably more hindered in accord with the enhanced rigidity of the blend (Figure 5.4). As a result, the diffusion length will be smaller, with an attendant decrease in the growth rate as seen in Figure 5.9, and the ultimate quenching of crystallization as seen in Figure 5.11. Furthermore, the presence of the small round, presumably, amorphous domains seen in the OM images of Figures 5.7 and 5.9, also lead to a local depletion of PCL in the "monolayer" form that can also inhibit the growth of sidebranches.

5.4. Conclusions

Π-A isotherm and BAM studies reveal that PCL is ideal for studying polymer crystallization within blends as Langmuir monolayers. In particular, the fact that PCL Langmuir films represent the thinnest possible uniform films for PCL, along with the relatively high compressibility (the A/W interface is a good solvent), low pressure for nucleation and growth of crystals ($\Pi_{c,PCL}$ ~ 11 $mN \cdot m^{-1}$), and room temperature crystallization observed for PCL are particularly amendable to blend studies because the isotherms are stable within the monolayer regime. The PCL/PtBA system presented here represents crystallization from a homogeneous blend with the formation of dendritic crystals during compression, a first for a polymer system at the A/W interface. These compositional dendrites exhibit morphologies that are comparable with diffusion-limited structures observed in polymer blends on solid substrates.[15, 17-26, 34] Moreover, the rheological properties of this blend are suitable for transferring the structures as LS films.

Analysis of these LS films by OM and AFM show the dendrites possess four symmetrically distorted {110} sectors and two {100} sectors. Within the {100} sector, the side branching angle is $\gamma \sim 49°$ and the branching is symmetric. In contrast, the side branching along the four trunks defining the boundaries between the {100} and {110} sectors is asymmetric with $\theta \sim 50°$ on the {110} side of the branch, and $\beta \sim 80°$ on the {100} side of the branch. Moreover, the crystal thicknesses, ~ 7 to 8 nm, are also comparable to the threshold film thickness below which dendritic structures are observed in PCL spincoated films on solid substrates.[14, 15] Hence, this study shows that Langmuir films provide a suitable framework for exploring dendritic crystal growth in thin films under ambient conditions where polymer degradation is not an issue by allowing one to vary both Π and T.